© 2019. Published by The Company of Biologists Ltd | Development (2019) 146, dev175257. doi:10.1242/dev.175257

RESEARCH ARTICLE

Mesenchymal proteases and tissue fluidity remodel the extracellular matrix during airway epithelial branching in the embryonic avian lung

James W. Spurlin[1], Michael J. Siedlik[1], Bryan A. Nerger[1], Mei-Fong Pang[1], Sahana Jayaraman[1], Rawlison Zhang[1] and Celeste M. Nelson[1,2,*]

ABSTRACT

Reciprocal epithelial-mesenchymal signaling is essential for morphogenesis, including branching of the lung. In the mouse, mesenchymal cells differentiate into airway smooth muscle that wraps around epithelial branches, but this contractile tissue is absent from the early avian lung. Here, we have found that branching morphogenesis in the embryonic chicken lung requires extracellular matrix (ECM) remodeling driven by reciprocal interactions between the epithelium and mesenchyme. Before branching, the basement membrane wraps the airway epithelium as a spatially uniform sheath. After branch initiation, however, the basement membrane thins at branch tips; this remodeling requires mesenchymal expression of matrix metalloproteinase 2, which is necessary for branch extension but for not branch initiation. As branches extend, tenascin C (TNC) accumulates in the mesenchyme several cell diameters away from the epithelium. Despite its pattern of accumulation, TNC is expressed exclusively by epithelial cells. Branch extension coincides with deformation of adjacent mesenchymal cells, which correlates with an increase in mesenchymal fluidity at branch tips that may transport TNC away from the epithelium. These data reveal novel epithelial-mesenchymal interactions that direct ECM remodeling during airway branching morphogenesis.

KEY WORDS: Jamming, Tissue morphodynamics, Mechanical stress

INTRODUCTION

Branching morphogenesis requires reciprocal signaling between the epithelium and mesenchyme in many organs, including the lung. Growth factors and other soluble signals expressed by the mesenchyme have been found to direct airway branching morphogenesis in both mammals (Bellusci et al., 1997; Lebeche et al., 1999; Min et al., 1998; Park et al., 1998; White et al., 2006) and birds (Moura et al., 2011). The relative balance of morphogens and their antagonists within the mesenchyme appears to influence the number, position and shape of epithelial branches (Gleghorn et al., 2012; Volckaert et al., 2013). Physical signals from the mesenchyme also influence the formation of epithelial branches during lung development. In the mouse, airway smooth muscle wraps the epithelium in a pattern that presages terminal bifurcation of the epithelium (Kim et al., 2015). Conversely, morphogens secreted by the epithelium and the mesothelium that surrounds the lungs direct the differentiation of the mesenchyme adjacent to the airways (Cohen et al., 2009; Kim et al., 2015; Mailleux et al., 2005; Warburton et al., 2005; White et al., 2006). For example, epithelial expression of sonic hedgehog (SHH) (White et al., 2006) promotes airway smooth muscle differentiation (Weaver et al., 2003). This reciprocal biochemical and mechanical signaling permits the epithelium and mesenchyme to sculpt each other into the final architecture of the lung.

In many branching programs, the extracellular matrix (ECM) is actively remodeled to facilitate the initiation, extension and shaping of branches (Kim and Nelson, 2012). The basement membrane is thought to influence epithelial growth and changes in branch shape (Bonnans et al., 2014; Daley and Yamada, 2013). Assembly of the basement membrane begins with polymerization of laminin at the cell surface (Hohenester and Yurchenco, 2013); laminin is expressed predominantly by the developing epithelium in the embryonic chicken (Chen et al., 1986) and rodent (Wu and Santoro, 1996) lungs. In addition to binding to cell-surface receptors, the laminin network is linked to the cell surface indirectly through interactions with heparan sulfate proteoglycans, including perlecan, which is expressed by mesenchymal cells in the chicken lung (Soulintzi and Zagris, 2007). These proteoglycans also connect the laminin network to type IV collagen as the basement membrane matures. Collagen IV is expressed by both the epithelium and mesenchyme in the embryonic rodent lung (Wu and Santoro, 1996) and may be similarly expressed in the bird. Remodeling of the mature basement membrane is required for branching morphogenesis of the epithelium in the mammary gland (Fata et al., 2004; Gomes et al., 2015; Wiseman et al., 2003) and kidney (Riggins et al., 2010). Similarly, basement membrane staining intensity is reduced at the tips of airway epithelial branches in both the mouse (Moore et al., 2005) and chicken (Abbott et al., 1991), but it is unclear whether this remodeling is required to specify sites of branch initiation or to permit branch extension.

In addition to a potential role for the basement membrane in airway branching, the mesenchyme itself contains several ECM proteins, including fibronectin (De Langhe et al., 2005) and tenascin C (TNC) (Gebb et al., 2005; Roth-Kleiner et al., 2004; Young et al., 1994), which facilitate epithelial-mesenchymal interactions during morphogenesis. For example, lungs from TNC-deficient mice form significantly fewer branches than wild-type lungs (Roth-Kleiner et al., 2004) and adding TNC to embryonic lung explants increases the number of epithelial branches (Gebb et al., 2005). Therefore, the current paradigm posits that mesenchymal expression of TNC results in the accumulation of this ECM protein at branch tips to

[1]Departments of Chemical & Biological Engineering, Princeton University, Princeton, NJ 08544, USA. [2]Molecular Biology, Princeton University, Princeton, NJ 08544, USA.

*Author for correspondence (celesten@princeton.edu)

C.M.N., 0000-0001-9973-8870

Received 1 January 2019; Accepted 16 July 2019

Development (2019) 146, dev175257. doi:10.1242/dev.175257

facilitate epithelial branching (Erickson and Bourdon, 1989). However, it is unclear how the expression and distribution of TNC are regulated during lung development.

In cultured fibroblasts, mechanical stress increases TNC expression (Chiquet-Ehrismann et al., 1994; Chiquet et al., 1996), which in turn suppresses cellular adhesion to the underlying substratum (Chiquet-Ehrismann and Chiquet, 2003; Midwood et al., 2004). Therefore, TNC may accumulate in specific locations in the developing lung as a result of mechanical stresses transmitted between the epithelium and the mesenchyme. Conversely, the local accumulation of TNC may impact the mechanical properties of the mesenchyme. TNC is a highly extensible protein (Cao and Li, 2006; Oberhauser et al., 1998) and provides elasticity and mechanical stability to tissues (Kimura et al., 2014; Midwood et al., 2016). Collectively, mesenchymal remodeling of the basement membrane and interstitial ECM may influence epithelial morphogenesis in the lung.

To define the relationship between ECM remodeling and airway branching morphogenesis, we characterized the distribution and intensity of the basement membrane and mesenchymal ECM prior to initiation and during extension of branches in the embryonic chicken lung. We found no evidence for basement membrane thinning or remodeling prior to or during branch initiation. After branch initiation, however, we found that the basement membrane is thinned at branch tips, which is necessary for branch extension. This basement membrane remodeling requires the activity of matrix metalloproteinases (MMPs), which are expressed in the mesenchyme. Additionally, as epithelial branches extend, TNC accumulates in the mesenchyme adjacent to branch tips. Surprisingly, however, TNC transcript is only expressed by the airway epithelium. We found that TNC expression requires signaling via focal adhesion kinase (FAK) and blocking FAK activation decreases branch extension. TNC accumulates in regions adjacent to extending epithelial branches where mesenchymal cells are deformed into elongated geometries. This change in mesenchymal cell shape and subsequent accumulation of mesenchymal TNC directly correlates with an increase in tissue fluidity within the mesenchyme around the branch tip, which may facilitate the transport of TNC protein through the mesenchyme. Our data therefore suggest that MMPs remodel the basement membrane, permitting branch extension. The extending epithelial branch compresses adjacent mesenchymal cells, which induces an increase in tissue fluidity and the transport of TNC from the epithelium into the mesenchyme. The resulting accumulation of TNC would be expected to change the local properties of the mesenchymal microenvironment and thereby influence epithelial branch extension in the embryonic chicken lung.

RESULTS

Airway epithelial branches initiate into undifferentiated mesenchyme in the embryonic chicken lung

Branching morphogenesis has long been appreciated to depend on reciprocal interactions between an epithelium and its surrounding mesenchyme (Wessells, 1970). In the early mammalian lung, the mesenchyme serves as a source of epithelial morphogens (Bellusci et al., 1997; Min et al., 1998; Morrisey and Hogan, 2010) and also differentiates into airway smooth muscle that wraps around the epithelium as it branches (Kim et al., 2015). We isolated lungs from chicken embryos between Hamburger and Hamilton stages (HH) 25-HH33 and stained for pan-cytokeratin (CK, airway epithelial marker) and α-smooth muscle actin (αSMA, smooth muscle marker). This analysis revealed that, from HH25 to HH28, the chicken airway epithelium branches in the absence of smooth muscle. In fact, no airway smooth muscle is detected until HH33, which is ∼72 h after branching initiates (Fig. 1A-O). These data suggest that, in the avian lung, a different set of epithelial-mesenchymal interactions governs branching morphogenesis.

Gene set enrichment analysis (GSEA) implicates cell-ECM interactions during branching morphogenesis

While mesenchymal cells remain undifferentiated during the early stages of epithelial morphogenesis, tenascin C (TNC) accumulates in the mesenchyme adjacent to extending branches, including branch tips and the distal tip of the primary bronchus (Fig. 1P-T). This pattern of TNC expression suggested a possible role for ECM remodeling during extension of the epithelium into the surrounding mesenchyme. This conclusion was supported by an unbiased analysis of genes that are differentially expressed during the branching process. We used RNA-Seq to perform differential gene expression analysis on transcripts isolated from lungs at embryonic day (E)5 (HH26-HH27) and E6 (HH28-HH29) (Fig. 2A,B). We identified gene ontology (GO) groups that were significantly enriched amongst the differentially expressed transcripts (Fig. 2B, $P<0.05$). These included several GO groups associated with lung development, including kinase signaling, Wnt signaling and epithelial differentiation.

As expected, this analysis also revealed several GO groups associated with cell-ECM adhesion. Examining the distribution of change in gene expression within each GO group revealed a significant difference when compared with the distribution of the total RNA-Seq dataset (Fig. 2C). Because integrins direct cellular responses to the ECM, we further validated genes associated with integrin-mediated signaling. We tested gene expression during branch initiation at E5 and as branches extend at E6. As predicted by the RNA-Seq, qRT-PCR analysis confirmed that β1-integrin (*ITGB1*) is downregulated during branching (Fig. 2D) whereas β3-integrin (*ITGB3*) is upregulated (Fig. 2E). The mechanical signaling protein focal adhesion kinase (FAK; *PTK2*) is elevated during branch extension (Fig. 2F), as is the mechanically regulated ECM protein TNC (Fig. 2G), which is consistent with our immunofluorescence analysis (Fig. 1P-T). Taken together, these data reveal that proteins associated with cell-ECM adhesion are differentially expressed during early lung development, suggesting a role for the ECM in mediating interactions between the epithelium and the mesenchyme in the embryonic chicken lung.

Branch initiation occurs independently of basement membrane remodeling

As branches extend in the embryonic chicken lung, the basement membrane thins at the branch tip (Abbott et al., 1991). However, it is unclear whether basement membrane thinning precedes branch initiation or whether basement membrane remodeling is required for branch extension. To define basement membrane dynamics during epithelial branching, we stained for laminin and perlecan at different stages of the morphogenetic process. At HH24, which corresponds to E4, the primary bronchus is a simple tube (Fig. 3A). At this stage, laminin is localized homogenously in a sheath around the basal surface of the bronchial epithelium (Fig. 3A,B). New branches initiate along the dorsal surface of the primary bronchus at precise positions over the subsequent days (Fig. 3A) (Gleghorn et al., 2012; Tzou et al., 2016). Because of this stereotypy, we can predict the region of the primary bronchus that will eventually initiate each branch. By HH25, the first branch (b1) consistently forms at a position 52% down the length of the primary bronchus (Fig. 3A,C).

Development (2019) 146, dev175257. doi:10.1242/dev.175257

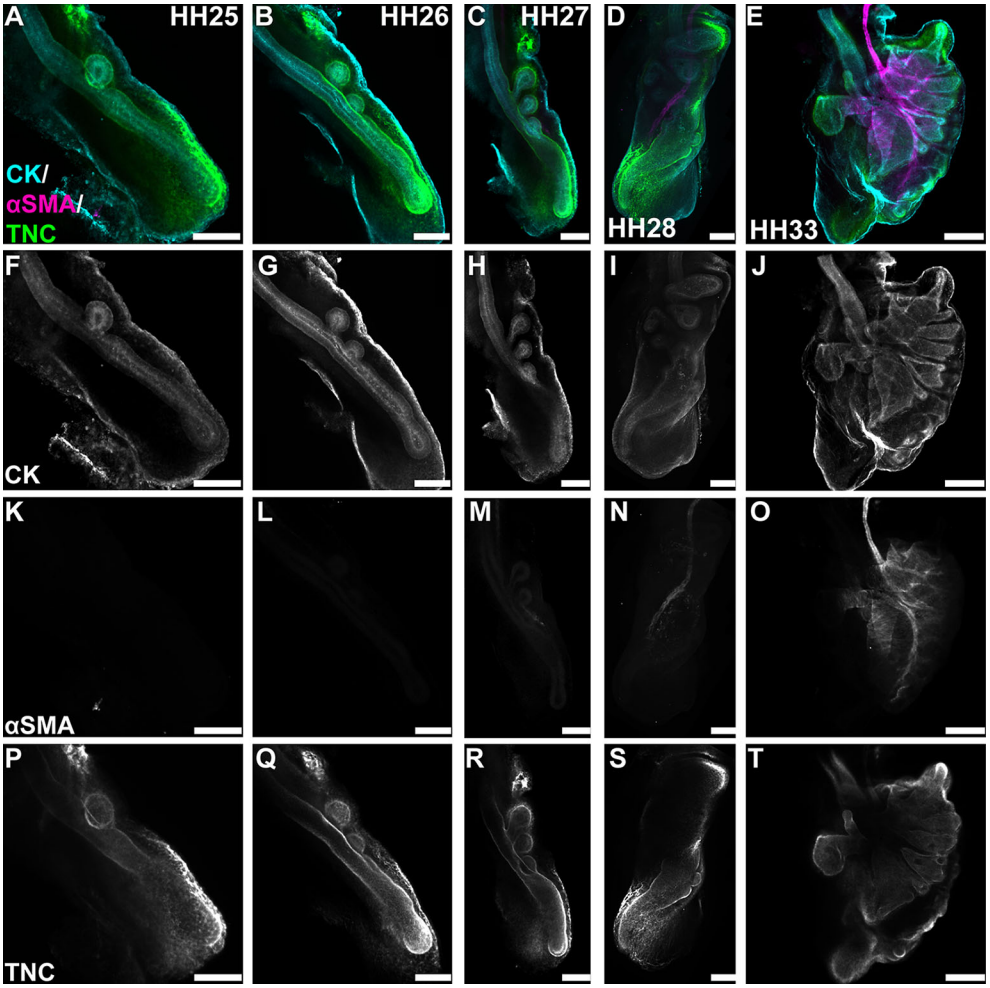

Fig. 1. Branching morphogenesis in the chicken lung occurs prior to the differentiation of airway smooth muscle. (A-E) Differentiation and ECM remodeling during branching morphogenesis were assessed by immunostaining HH25-HH33 lungs for cytokeratins (CK; cyan) to label the airway epithelium and mesothelium, and αSMA (magenta) to label airway smooth muscle. Changes in mesenchymal ECM composition were monitored by immunostaining for tenascin C (TNC; green). (F-J) Airway branches begin forming at HH25 and continue to extend through HH33. (K-O) Airway smooth muscle is not observed until HH33. (P-T) The mesenchyme around the tips of growing branches is enriched in TNC beginning at HH25. Scale bars: 150 µm in A-D,F-I,K-N,P-S; 300 µm in E,J,O,T.

At HH24, immediately prior to the emergence of b1, we found that the intensity of laminin staining is uniform along the dorsal surface of the airway epithelium, with no apparent decrease in signal in the region where b1 will eventually form (*b1, Fig. 3B,E). After b1 forms, the intensity of the laminin signal decreases at the branch tip (Fig. 3C, arrow) and simultaneously increases along the branch stalk (Fig. 3C, arrowhead). We observed similar changes in the distribution of the basement membrane protein perlecan (Fig. S1).

Normalizing the staining intensity of laminin to that along non-branched regions highlights changes in the basement membrane around b1 during branch initiation (Fig. 3E). As b1 extends through HH28, the distribution of laminin is maintained, with enhanced signal along the branch stalk (Fig. 3D, arrowheads) and decreased signal at the branch tip (Fig. 3D, arrow; F). To better understand how the distribution of laminin changes dynamically during branch extension, we measured the fraction of the branch surface that shows a decrease in laminin staining intensity (when compared with non-branching regions of the primary bronchus, Fig. 3G). We found that the percentage of the branch surface with depleted laminin decreases as the branch extends. However, the area of the branch tip with depleted laminin increases during branch extension. Collectively, these data show that the basement membrane does not thin prior to branch initiation. Therefore, basement membrane staining intensity cannot be used to predict future branch sites. However, laminin and perlecan are depleted at the tips of branches after branch initiation, suggesting that the basement membrane is remodeled during branch extension.

Matrix metalloproteinases remodel the basement membrane to promote airway extension

Matrix metalloproteinases (MMPs) influence branching morphogenesis by remodeling the ECM in many organs (Lu et al., 2011). RNA-Seq analysis also detected the expression of several MMPs during crucial stages of airway branching morphogenesis, including upregulation of MMP2 and downregulation of membrane-associated MMP15, MMP16, MMP17 and MMP24. To determine whether MMP activity is required for thinning of the basement membrane during airway branching in the embryonic chicken lung, we isolated lungs at HH26 and cultured them in the presence of the broad-spectrum MMP inhibitor, GM6001. Branch initiation is not significantly affected at low concentrations of GM6001 (5 or 10 µM) and still occurs at higher concentrations (20 µM, n=10/11 explants, Fig. 4A,B). However, inhibiting MMP activity causes a reduction in branch extension (Fig. 4A,C) and in the projected area of b1 when compared with controls (Fig. 4D), without affecting proliferation of the airway epithelium (Fig. S2). These data suggest that MMP activity is necessary for the extension of branches after they have formed. To determine whether MMP activity is required for depletion of the basement membrane during branch extension, explants cultured in the presence of GM6001 were stained for laminin and analyzed as described above. Similar to the distribution *in vivo*, control explants show reduced laminin at branch tips (Fig. 4E, arrow) and an increase along branch stalks (Fig. 4E, arrowhead). Explants cultured in the presence of GM6001 also exhibit increases in laminin intensity along the stalk of b1 (Fig. 4F,G, arrow). However, treatment

Development (2019) 146, dev175257. doi:10.1242/dev.175257

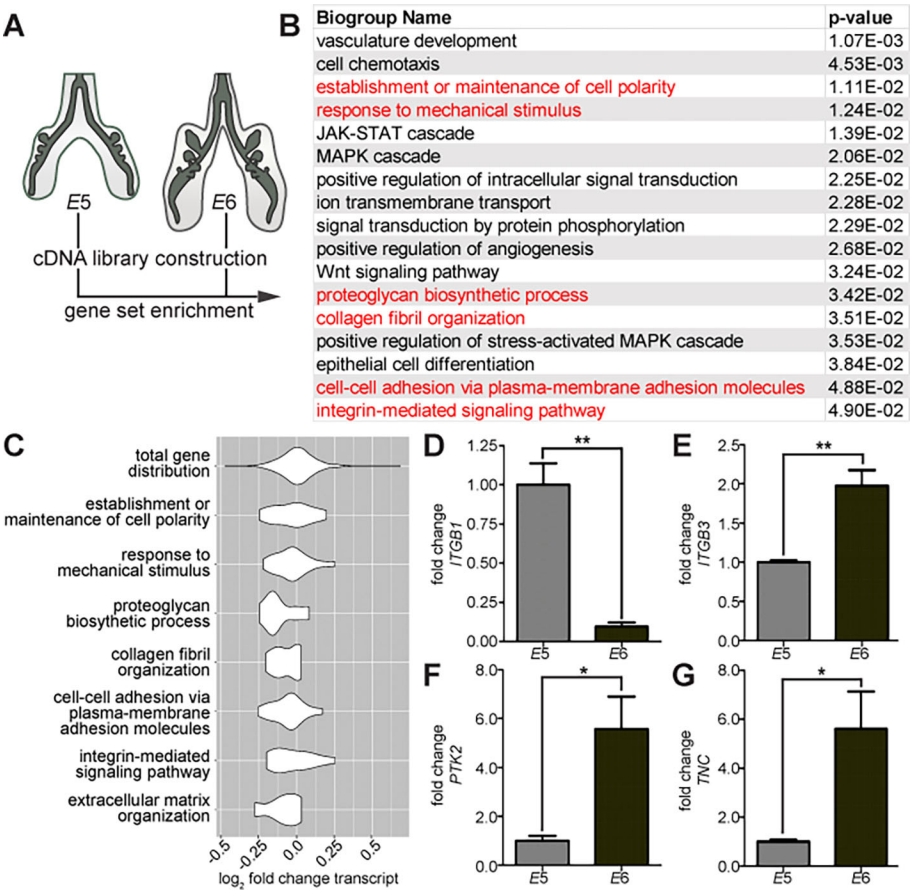

Fig. 2. Gene expression analysis during branching morphogenesis of the embryonic chicken lung. (A) Gene expression analysis was performed by comparing differential levels of transcripts between lungs collected at E5 (HH25-27) and E6 (HH28-29). (B) GO analysis identified several biogroups that are enriched (P<0.05). The full enriched GO list is available in Table S1. (C) Violin plots were generated to show the distribution of differentially expressed genes within GO groups relative to the distribution of all genes within the RNA-Seq dataset. (D) Several ECM-related genes found to be differentially expressed were validated, including integrins *ITGB1* and *ITGB3*, FAK (*PTK2*), and tenascin C (*TNC*). Data are mean±s.e.m. of n=3 independent experiments. *P<0.05, **P<0.01 using Student's t-test.

with GM6001 prevents laminin depletion at the tip of b1 (Fig. 4F-H). We found similar effects in explants treated with another broad-spectrum MMP inhibitor, batimastat (Fig. S3A-C). These data show that MMPs remodel the basement membrane at the tips of epithelial branches to promote branch extension.

To determine which MMPs are responsible for remodeling of the ECM around the branch tip, we isolated lungs from HH28-HH29 chicken embryos and examined the expression of MMPs associated with mammalian lung development (MMP2 and MMP14) as well as MMP9, which is associated with remodeling of the ECM in the adult mammalian lung. Using quantitative RT-PCR analysis, we found significantly higher expression of MMP2 than MMP9 or MMP14 at this stage of development (Fig. 4I). To determine which cells express MMP2, we conducted *in situ* hybridization analysis on lungs isolated from HH25-HH28 embryos. MMP2 transcript is distributed throughout the lung mesenchyme, specifically adjacent to the primary bronchus (Fig. 4J). To determine whether MMP2 is required for remodeling the basement membrane, we cultured lung explants from HH26 embryos with an MMP2-specific inhibitor, ARP100, and measured the staining intensity of laminin. Treatment with ARP100 results in a reduction in basement membrane thinning at branch tips (Fig. 4K), indicating that MMP2 is required to degrade this ECM during branch extension. Moreover, explants treated with ARP100 have shorter branches and reduced projected area, but the epithelium shows no changes in proliferation (Fig. S2) and still initiates new branches (Fig. S3D-F). Treating explants with a second MMP2-specific inhibitor yielded similar results (Fig. S3G-K). These data suggest that mesenchymal MMPs, specifically MMP2, degrade the basement membrane and that this process is required for the epithelial branch to extend into the surrounding mesenchyme.

The mesenchymal ECM protein TNC is expressed by the airway epithelium during branch extension

That basement membrane remodeling is required for branch extension suggests that this ECM acts as a barrier to epithelial interactions with the mesenchyme. As the epithelium extends, the mesenchymal ECM might also be remodeled. TNC is a mechanically regulated protein that is associated with an increase in tissue elasticity (Midwood et al., 2016). TNC protein has been localized to the mesenchyme of the developing lung (Abbott et al., 1991). In other organs, TNC is expressed by endothelial cells within the blood vessel walls and is associated with vessel maturation (Imanaka-Yoshida et al., 2014). To determine whether the pattern of TNC protein is associated with concurrent development of blood vessels around the airway epithelium, we intravenously injected fluorescently labeled lectin into the extra-embryonic vasculature of the developing embryo *in ovo* to label the lung vasculature (Fig. S4). We found that blood vessels wrap around the airway epithelium at HH24, before the initiation of epithelial branches or appearance of TNC protein within the mesenchyme. This wrapping continues during the initiation of epithelial branching at HH25; however, very little TNC is observed within the mesenchyme at this time (Fig. S4B). TNC protein begins to accumulate within the mesenchyme as epithelial branches extend through the vascular network (Fig. S4D), which results in very few blood vessels around the branch tip. These data suggest that the pattern of TNC accumulation within the mesenchyme is independent of mature blood vessels.

Development (2019) 146, dev175257. doi:10.1242/dev.175257

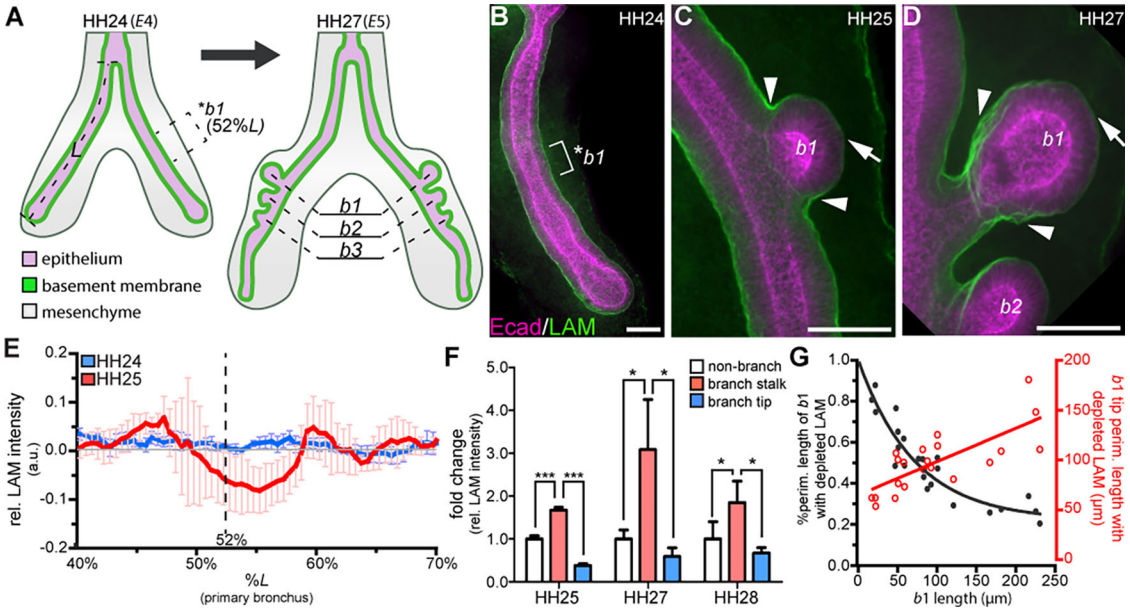

Fig. 3. Basement membrane thinning occurs after branch initiation and during branch extension. (A) Schematic of embryonic chicken lung showing the stereotyped position at which b1 initiates (52%L, where L is length from the tracheal fork to the distal tip of the primary bronchus). (B-D) Staining for the basement membrane protein laminin (LAM, green) and for E-cadherin (Ecad, magenta) in the airway epithelium (B) prior to b1 initiation, (C) during b1 initiation and (D) during b1 extension. Laminin intensity increases at branch stalk (arrowheads, C,D) and decreases at branch tip (arrows, C,D). *b1 indicates the region (brackets) where b1 will form. (E) Plot of laminin intensity at b1 before (blue, HH24) and during (red, HH25) branch initiation; *n*=3-5 independent experiments. (F) Mean laminin staining intensity in the branch stalk (arrowheads in C,D) and branch tip (arrows in C,D) normalized to non-branching regions; *n*=3 independent experiments. (G) Plot of the percentage of cross-sectional b1 surface (black) and the size of the b1 surface (red) that shows depletion of laminin as a function of b1 length; *n*=20 lung explants. Data are mean±s.d. **P*<0.05, ****P*<0.001 using one-way ANOVA with Tukey's post-hoc test. Scale bars: 40 µm.

To determine which cells express TNC, we performed *in situ* hybridization analysis on lungs isolated from HH25-HH36 embryos (Fig. 5A, Fig. S5). Although TNC protein accumulates in the mesenchyme (Fig. 1P-T), we found that TNC transcript is localized exclusively to airway epithelial cells, with the highest expression within the cells at the tips of the extending branches (Fig. 5A-D), consistent with studies of older lungs (Koch et al., 1991). When we dissected the mesenchyme away from the epithelium and used qRT-PCR to measure levels of TNC transcript, we found that the epithelium expresses ∼20-fold more TNC than does the mesenchyme (Fig. 5E-G). Furthermore, when mesenchyme-free airway epithelium was cultured within Matrigel, this tissue expressed both TNC transcript as well as protein (Fig. S6). Immunofluorescence analysis revealed that TNC protein accumulates in the mesenchyme adjacent to the tips of branches beginning at HH25 and increases in intensity as branches extend through HH29 (Fig. 5H-L). This analysis also showed synthesis of TNC protein within epithelial cells at the branch tip (Fig. 5I, arrow) located adjacent to where it accumulates within the surrounding mesenchyme (Fig. 5I, arrowhead). TNC is absent from the mesenchyme surrounding nascent branches (Fig. 5J-L, asterisks), but increasing amounts of TNC appear as epithelial branches extend (Fig. 5J-L, arrowheads).

These data show that synthesis of TNC is restricted to the airway epithelium in the embryonic chicken lung, despite its accumulation in the mesenchyme. In cultured cells, TNC expression is regulated by the mechanosensory protein FAK (McKean et al., 2003). Consistently, we found activated FAK (pFAK) localized to the basal region of the airway epithelium (Fig. 6A). To determine whether FAK activation is necessary for TNC expression, we cultured explanted lungs in the presence of the FAK inhibitor PF-573228 (Slack-Davis et al., 2007). We found that as the concentration of PF-573228 increased, the levels of TNC protein within the airway epithelium of the lung decreased (Figs 5F,G and 6B-D). Explants treated with the highest concentration of PF-573228 (1 µM) also exhibit significantly shorter branches (Fig. 6E) but inhibiting FAK had no effect on proliferation of the airway epithelium (Fig. S2). *In situ* hybridization analysis revealed that FAK activation is required for expression of TNC transcript by the airway epithelium (Fig. 6F). Furthermore, qRT-PCR analysis revealed a significant reduction in TNC transcript levels in explants treated with FAK inhibitor (Fig. 6G). These data show that epithelial cells at the tips of the branches activate FAK and synthesize TNC, which is transported into the adjacent mesenchyme during branch extension.

Lung mesenchymal cells change shape and increase local tissue fluidity as epithelial branches extend

Although TNC is synthesized by the epithelium, the protein accumulates up to 10 cell diameters away in the mesenchyme adjacent to extending branches. Each TNC monomer is 180-240 kDa and assembles into hexamers as it is exocytosed by the cell (Redick and Schwarzbauer, 1995). Finite element method-based analysis suggests that the diffusion of a protein of this size is limited (Fig. S7); consistently, immunofluorescence analysis revealed a tight association between TNC protein and the basal surface of the epithelium in mesenchyme-free culture (Fig. S6). However, we observed TNC protein at distances greater than 50 µm from the basal surface of the airway epithelium. We therefore hypothesized that TNC may be transported through the mesenchyme by convective flow within the tissue surrounding the tip of the epithelial branch. To test this hypothesis, we measured the relative fluidity of the mesenchyme in the embryonic lung. We injected 1 µm diameter fluorescent beads into the mesenchyme and monitored

Development (2019) 146, dev175257. doi:10.1242/dev.175257

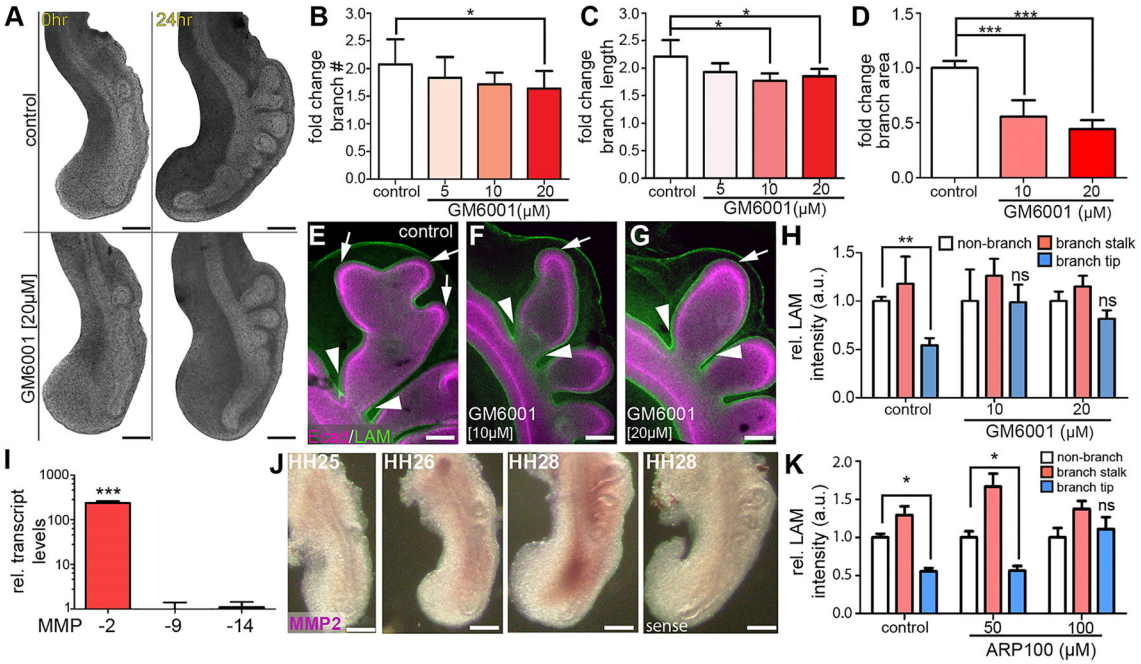

Fig. 4. MMP activity is required for branch extension but not branch initiation. (A) Bright-field images of control and GM6001-treated (20 µM) chicken lung explants after 24 h of culture. (B-D) After the 24 h culture period, fold-change in branch (B) initiation, (C) extension and (D) projected area were measured; *n*=4-6 independent experiments for B-D. (E-G) Remodeling of basement membrane was monitored by staining for laminin (LAM; green) in (E) control explants, as well as in (F,G) explants cultured in the presence of GM6001. Epithelial cells were stained for E-cadherin (Ecad, magenta). Arrows and arrowheads indicate regions of basement membrane thinning and accumulation, respectively. (H) Relative staining intensities were quantified as described in Fig. 2; *n*=4-6 independent experiments. (I) qRT-PCR analysis for relative MMP expression in HH28 lungs; *n*=3 independent experiments. (J) *In situ* hybridization for MMP2 in HH25-HH28 lungs. (K) Relative staining intensity of laminin in lung explants treated with the MMP2-specific inhibitor ARP100; *n*=4-6 independent experiments. Data are mean±s.d. **P*<0.05, ***P*<0.01, ****P*<0.001 (one-way ANOVA with Tukey's post-hoc test). Scale bars: 200 µm in A,J; 50 µm in E-G.

their movement directly in front of an extending branch or adjacent to non-branching epithelium (Fig. 7A,B). Time-lapse video tracking revealed that beads injected adjacent to branch tips exhibit movements that are greater than diffusion, indicated by a mean squared displacement (MSD) slope >1.0 (Fig. 7C). In contrast, beads injected adjacent to non-branching epithelium appear to move diffusively (MSD slope ∼1.0). Consistently, beads injected adjacent to extending branches move significantly farther than those adjacent to non-branching epithelium (Fig. 7D).

To determine why the mesenchyme adjacent to extending branches shows increased fluidity, we stained for F-actin to visualize individual mesenchymal cells (Fig. 7E). Quantitative imaging analysis of confocal sections revealed that mesenchymal cells adjacent to the tips of epithelial branches are more elongated than those adjacent to non-branching epithelium (Fig. 7E,F). When we mapped the aspect ratio of mesenchymal cells as a function of position around epithelial branches of increasing lengths (Fig. 7G), we found that cells with the highest aspect ratios are restricted to the mesenchyme adjacent to the leading edge of the branch (between 0.35 and 0.65 of the total branch surface). This suggests that the extending airway epithelium pushes into the surrounding mesenchyme and compresses the mesenchymal cells. Taken together, these data show that mesenchymal cell elongation and increased fluidity are unique to the mesenchyme adjacent to the airway branch tip. This local increase in tissue fluidity could transport TNC from the epithelium and into the mesenchyme, thus yielding the staining patterns observed during branch extension.

Changes in cellular aspect ratio have been correlated with increases in the fluidity of two-dimensional (2D) epithelial cell sheets, both experimentally and computationally (Bi et al., 2016; Manning et al., 2010; Park et al., 2015). In particular, elongated epithelial cells with a shape factor ($q=P/\sqrt{A}$)>3.81 have been found to undergo a solid-to-liquid, or unjamming, transition (Bi et al., 2016). Although shape factor appears to predict unjamming and an increase in tissue fluidity for 2D epithelial monolayers, it remains unclear whether such a parameter is predictive for three-dimensional (3D) mesenchymal tissues *in vivo*. To begin to assess its relevance, we calculated a 'projected shape factor' from our quantitative imaging data and found that this parameter also correlates with our bead displacement measurements. Specifically, we found that mesenchymal cells adjacent to extending branches have a projected shape factor significantly larger than those adjacent to the non-branching epithelium (Fig. 7H,I). Moreover, these changes in cell shape directly correspond to the accumulation of TNC in the mesenchyme surrounding the extending airway epithelium (Fig. 7J-M). These data identify a specific change in the shape of mesenchymal cells surrounding the airway epithelium, which corresponds to increased fluidity within the mesenchyme as branches extend. This motion within the mesenchyme may facilitate the transport of TNC protein and subsequent extension of the epithelial branch.

DISCUSSION

Reciprocal interactions between an epithelium and its surrounding mesenchyme are well appreciated to instruct morphogenesis. For example, grafting lung mesenchyme to non-branching epithelium induces branch formation in the trachea (Wessells, 1970), suggesting that mesenchymally derived factors drive branching morphogenesis in the lung. This seminal work prompted the use of mesenchyme-free cultures of lung epithelium to test the capacity of

Development (2019) 146, dev175257. doi:10.1242/dev.175257

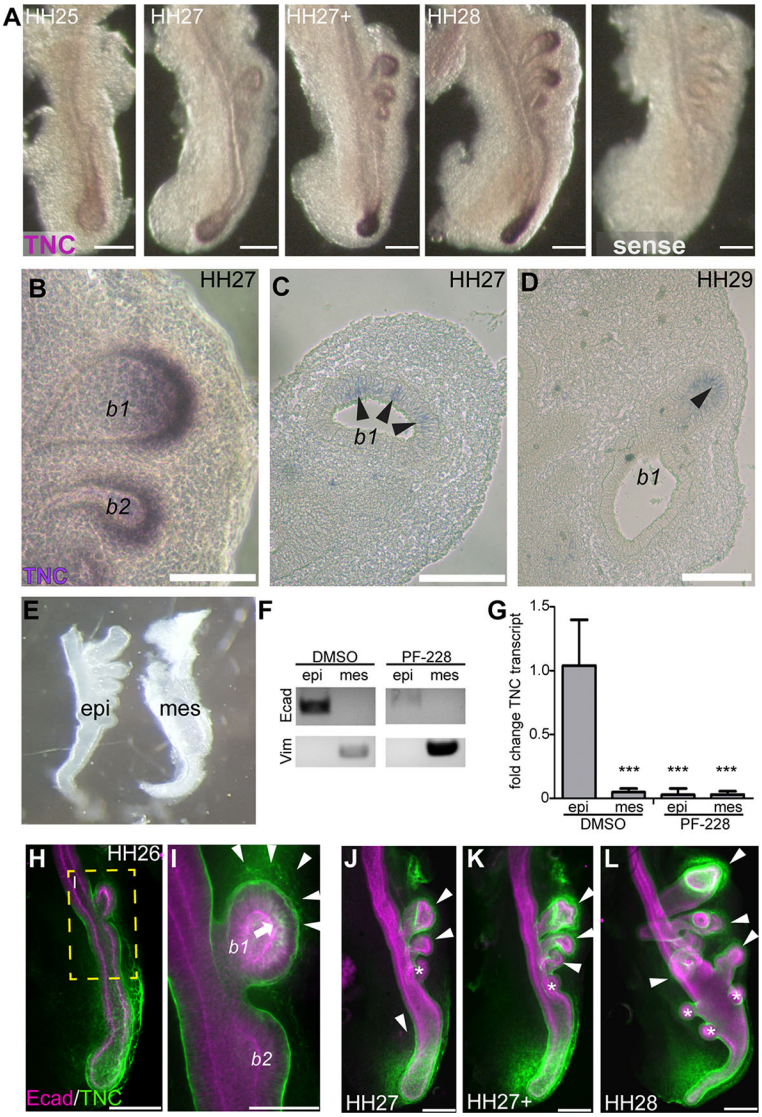

Fig. 5. TNC is expressed by airway epithelial cells and accumulates in the adjacent mesenchyme. (A) *In situ* hybridization for TNC in lungs isolated from HH25-HH28 embryos. TNC is expressed by the epithelium at the tips of airway branches. (B) Higher magnification image of *in situ* hybridization for TNC in HH27 lung. (C,D) *In situ* hybridization for TNC in sections from HH27 (C) and HH29 (D) lungs. Arrowheads indicate TNC expression in the epithelium. (E) Separation of the mesenchyme (mes) from the epithelium (epi) to measure relative levels of TNC transcript in each tissue compartment. (F) RT-PCR for E-cadherin (Ecad) and vimentin (vim) in separated epithelial and mesenchymal compartments. (G) qRT-PCR analysis for TNC transcript in the separated epithelial and mesenchymal compartments; n=3 independent experiments. (H-L) TNC protein (green) during airway branching. Airway epithelial cells were stained for E-cadherin (Ecad, magenta). TNC is found in the mesenchyme around b1 by HH26 (arrowheads in I). TNC staining is found in the airway epithelial cells in branch tips (arrow in I) and increases in the mesenchyme adjacent to branch tips during extension (arrowheads in J-L). TNC is absent from the mesenchyme proximal to newly formed branches (asterisks in J-L). I is a higher magnification view of the boxed area in H. Data are mean±s.d. ***P<0.001 using one-way ANOVA with Tukey's post-hoc test. Scale bars: 200 µm in A,C,D; 100 µm in B.

soluble, mesenchymally secreted growth factors to induce epithelial branching (Park et al., 1998; Bellusci et al., 1997; Weaver et al., 2003). Such mesenchyme-free systems identified specific fibroblast growth factors (FGFs) as branch inducers and established a paradigm wherein spatially patterned expression of FGF within the mesenchyme directs the stereotyped epithelial branching observed in the lung (Cardoso and Lu, 2006; Guo et al., 2014; Iber and Menshykau, 2013; Morrisey and Hogan, 2010). However, although FGF signaling is required for lung formation and branching of the airway epithelium, ubiquitous expression of FGF10 in developing lungs within FGF10-deficient mice restores normal branching patterns (Volckaert et al., 2013). These data suggest that additional mesenchymally derived signals are required to direct stereotyped branching morphogenesis in the lung. Mechanical forces within the mesenchyme shape growing epithelia and can influence airway epithelial branching (Varner et al., 2015). The differentiation of smooth muscle within the mesenchyme is associated with epithelial folding in the mammalian lung (Danopoulos et al., 2018; Kim et al., 2015) and epithelial buckling in the chicken gut (Shyer et al., 2015). Our data now suggest a crucial role for ECM remodeling in epithelial-mesenchymal interactions during branching morphogenesis of the embryonic chicken lung.

In epithelial tissues, the basement membrane provides both mechanical and biochemical signals that direct cell behavior. Concurrent with epithelial branching, the surrounding basement membrane is thinned at the tips of extending branches. It has been proposed that the basement membrane is in a state of isometric tension and that this ECM layer can constrain branching of the airway epithelium (Moore et al., 2005). Such a model assumes a requirement for localized degradation to increase compliance of the basement membrane, which would promote branch initiation. Our data show that thinning of the basement membrane does not precede branch initiation in the developing chicken lung. Instead, basement membrane thinning is restricted to the leading edges of extending branches after they have already initiated off the primary bronchus. Thinning of the basement membrane requires the activity of MMPs that are expressed in the mesenchyme. Remodeling of the epithelial basement membrane and subsequent branch extension thus requires signaling from the mesenchyme.

Inhibiting MMP activity results in shorter epithelial branches without affecting epithelial proliferation (Fig. S2) or TNC synthesis (Fig. S8). There are two possible explanations for this observation. First, the basement membrane may physically constrain the growing epithelium during lung morphogenesis. Therefore, basement membrane remodeling at the tip of the branch may promote

Development (2019) 146, dev175257. doi:10.1242/dev.175257

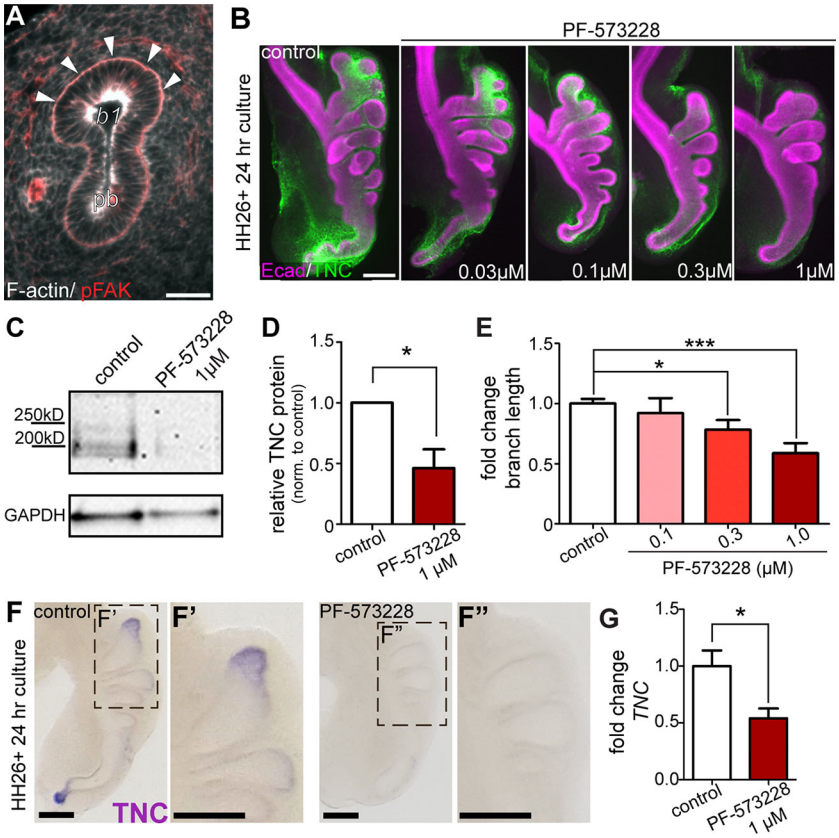

Fig. 6. FAK is required for TNC expression and branch extension. (A) Histological section shows pFAK (red, arrowheads) localized to the basal surface of the airway epithelium. (B) Explants isolated at HH26 were cultured for 24 h in the presence of increasing concentrations of the FAK inhibitor PF-573228. TNC distribution around airway epithelial branches was observed with immunostaining (TNC, green; Ecad, magenta). Explants cultured in the presence of PF-573228 were compared with untreated controls. (C) Immunoblotting for TNC was performed on protein extracts isolated from HH26 lung explants cultured for 24 h and (D) fold change of TNC band intensity was quantified in PF-573228-treated explants relative to control; n=3 independent experiments. (E) Fold-change in branch extension of explants treated with increasing concentrations of PF-573228 for 24 h; n=4 or 5 independent experiments. (F-F″) *In situ* hybridization for TNC transcript in control and PF-573228-treated lung explants. (G) qRT-PCR analysis of explants cultured in the presence of PF-573228 for 24 h; n=3 independent experiments. Data are mean±s.d. *P<0.05, ***P<0.001 using (D,G) Student's t-test or (E) one-way ANOVA with Tukey's post-hoc test. Scale bars: 40 µm in A; 200 µm in B,F.

extension of the epithelium into the mesenchyme, similar to other branched epithelia such as the mammary (Wiseman et al., 2003) and salivary (Harunaga et al., 2014) glands. Second, basement membrane proteins may provide biochemical signals that direct epithelial cell behavior. For example, proteoglycans present in the basement membrane, such as perlecan, can sequester and control the release of growth factors that are crucial for branching morphogenesis. During development of the salivary gland, heparanase-mediated cleavage of perlecan modulates the availability of FGF10 to submandibular epithelial cells (Patel et al., 2007). We found that both laminin and perlecan were depleted at the tips of extending branches; it is possible that this basement membrane remodeling releases growth factors to promote epithelial growth. In addition to basement membrane thinning at the tip of the branch, we observed a significant thickening of basement membrane along the stalk. Considering the mechanical and biochemical roles of the basement membrane described above, we hypothesize that both constraint of epithelial growth and sequestration of growth factors may be altered during branch extension.

As epithelial branches extend, the adjacent mesenchymal cells become elongated, increase tissue fluidity and transport TNC from the epithelial surface to deeper within the mesenchyme. The expression of epithelial-derived TNC requires signaling from the mechanosensory protein, FAK, which is activated in epithelial cells at the tips of extending branches. Inhibiting FAK blocks the synthesis of TNC but has no effect on mesenchymal cell shape (Fig. S2). Epithelial cells within the branch tip also undergo apical constriction, which increases tensile loading of their basal surfaces (Kim et al., 2013) and may be sufficient to activate FAK. Given that apical constriction of the airway epithelium is required for branch initiation in the embryonic chicken lung (Kim et al., 2013), we hypothesize that FAK may also regulate airway branching by modulating epithelial cell contractility. Consistent with this hypothesis, fewer branches form in the presence of high concentrations of the FAK inhibitor (Fig. 6B, Fig. S2). TNC is often expressed in tissues under mechanical load, such as compressed tendons (Mehr et al., 2000) and stretched skeletal muscle (Fluck et al., 2000). Our data therefore suggest that TNC expression in the epithelium of the embryonic lung is promoted by mechanical activation of FAK at airway branch tips.

TNC is found at the epithelial-mesenchymal interface in many organs during development (Erickson and Bourdon, 1989), including the mesenchyme of growing intestinal villi (Belanger and Beaulieu, 2000), the stroma of the embryonic mammary gland (Inaguma et al., 1988) and the metanephric mesenchyme of the kidney (Aufderheide et al., 1987). Surprisingly, TNC protein is not detected in these tissues until the epithelial cell layer has impacted the geometry of the adjacent mesenchyme. For example, TNC is prominent in the kidney mesenchyme only after epithelial tube ingression (Aufderheide et al., 1987), suggesting epithelial-mesenchymal interactions might promote accumulation of TNC in the mesenchyme. Moreover, grafting kidney epithelial cells into undifferentiated, TNC-free mesenchyme results in the accumulation of TNC protein (Aufderheide and Ekblom, 1988), suggesting that epithelial cells are required for TNC production. In contrast to the current paradigm, which suggests that epithelial cells provide an inductive cue to stimulate mesenchymal expression of TNC (Erickson and Bourdon, 1989), our data show that TNC is synthesized by airway epithelial cells at the branch tips and is transported into mesenchyme. It will be interesting to determine whether this classical 'mesenchymal ECM' is also expressed by the epithelium in other organ systems.

TNC is a large hexameric protein, which our finite element modeling predicts would show limited diffusion from the surface of

Development (2019) 146, dev175257. doi:10.1242/dev.175257

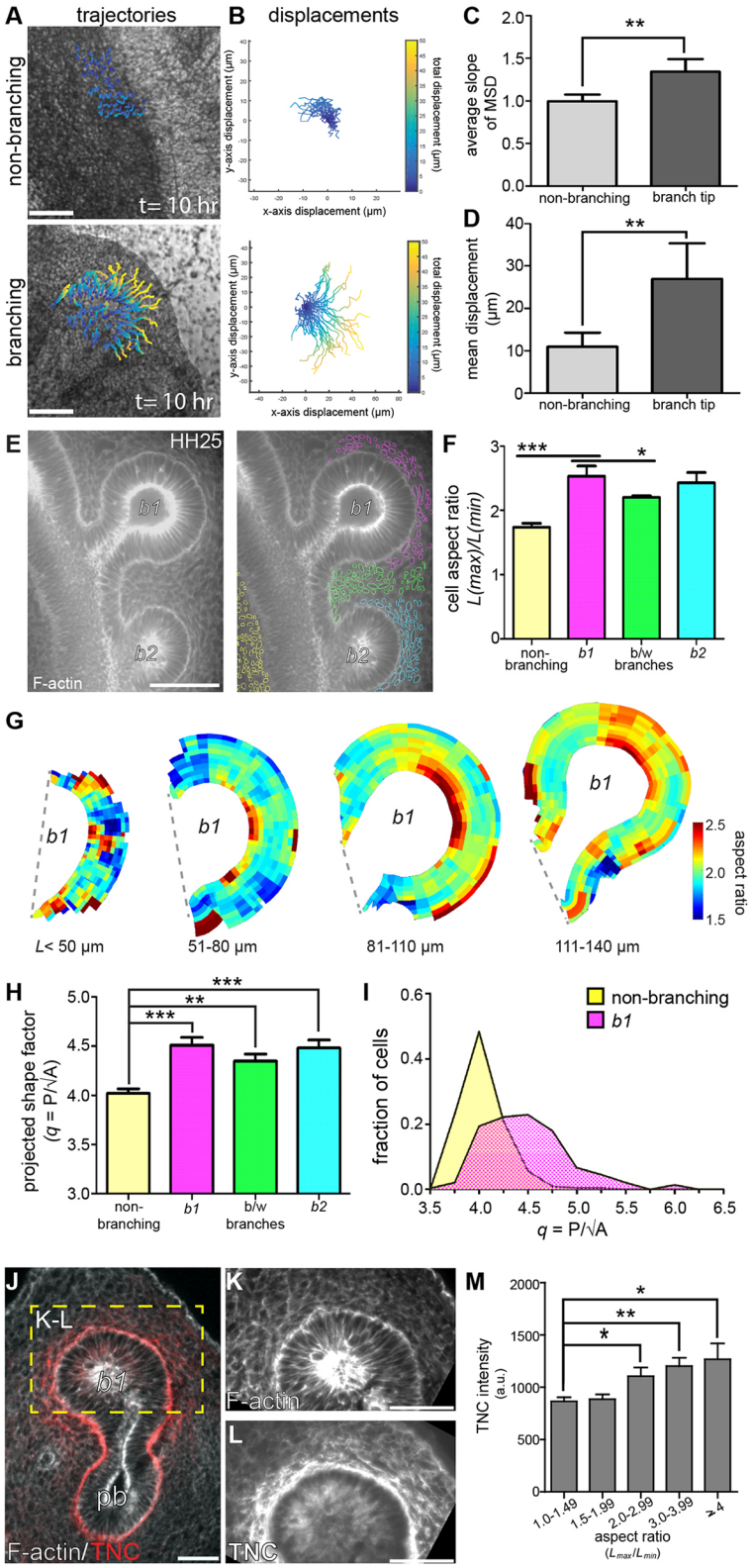

Fig. 7. Mesenchyme surrounding branch tips exhibits increased fluidity, cell deformation and TNC protein accumulation. (A) Fluorescent beads were injected into the lung mesenchyme adjacent to non-branching and branching airway epithelium. Bead trajectories were generated from 10 h long time-lapse videos. (B) Bead displacements were plotted with the starting position (t=0) at the origin. (C) Average mean squared displacement (MSD) and (D) total displacement of each bead (over 10 h of imaging) were calculated; *n*=4 or 5 independent experiments for C,D. (E) Mesenchymal cell shapes were visualized by staining for F-actin (gray) and were segmented by location. (F) Mean aspect ratio of cells in each respective spatial location (yellow, non-branching; pink, b1; green, between b1 and b2; cyan, b2) around extending branches; *n*=4 independent experiments. (G) Composite heat maps of mesenchymal cell aspect ratio around the tip of b1 during branch extension. (H) Projected shape factor of mesenchymal cells in each respective spatial location; *n*=3-5 independent experiments. (I) Distribution of cells binned by projected shape factor in mesenchyme adjacent to non-branching (yellow) and b1 (pink) epithelial branches; *n*=4 independent experiments. (J) TNC and F-actin were stained in histological sections to correlate TNC protein localization to mesenchymal cell deformation (red, TNC; gray, F-actin; pb, primary bronchus). (K,L) Cell shapes were found in the mesenchyme (K) and the coordinates of cells identified were used to survey TNC staining intensity (L). (M) Mean relative TNC intensity increases as mesenchymal cells increase in deformation; *n*=3 independent experiments. Data are mean±s.d. (C,D,F,H) or mean±s.e.m. (M). **P*<0.05, ***P*<0.01, ****P*<0.001 using (C,D) Student's *t*-test or (F,H,M) one-way ANOVA with Tukey's post-hoc test. Scale bars: 40 μm in E,J; 50 μm in A,K,L.

the epithelial branch. However, we observe TNC in the mesenchyme greater than 50 μm away from the basal surface of the epithelium. One possible explanation for this observed distribution of TNC is that the mesenchyme adjacent to extending branches is more fluid than the mesenchyme near non-branching epithelium. Indeed, changes in tissue fluidity have been observed in other organs during embryonic development. During elongation of the vertebrate body axis, the notochord extends (Kimmel et al., 1995) and imparts mechanical stress (Serwane et al., 2017) on the adjacent mesoderm, which deforms mesodermal cells. These changes in mesodermal cell geometry drive a solid-to-fluid transition within the mesoderm, which reduces the viscosity and

Development (2019) 146, dev175257. doi:10.1242/dev.175257

increases the relative fluidity of the tissue directly in front of the extending notochord (Mongera et al., 2018). During epithelial morphogenesis in the lung, branches extend into the mesenchyme and deform the adjacent cells. This deformation may result from mechanical compression of the mesenchyme by the extending epithelium. Similar to what occurs in the vertebrate mesoderm during body axis elongation, the pulmonary mesenchyme becomes fluid as airway epithelial branches elongate, which may transport an epithelial-derived mesenchymal protein (TNC) into the tissue. Several cell types within the mesenchymal compartment, including endothelial cells, express receptors for TNC (Orend and Chiquet-Ehrismann, 2006) and could bind to and facilitate the transport of this protein as they migrate. However, branch extension may also promote interstitial fluid flow, which could transport TNC by advection.

The relative abundance of TNC and other ECM proteins within the mesenchyme could impact branching morphogenesis in several ways. First, cells activate integrin signaling and mechanotransduction pathways when they adhere to fibronectin (Sun et al., 2016). However, TNC directly competes with fibronectin-integrin interactions, resulting in destabilization of focal adhesion complexes (Midwood and Schwarzbauer, 2002) and reduced cell adhesion to fibronectin (Chiquet-Ehrismann et al., 1988). This could alter cellular sensitivity to stresses during morphogenesis (Sarasa-Renedo et al., 2006). TNC may also affect the bulk mechanics of the pulmonary mesenchyme. Single-molecule mechanical testing has revealed that although fibronectin is the most extensible ECM protein currently known (Klotzsch et al., 2009), it has greater tensile strength and slower mechanical recovery after stretch than does TNC (Oberhauser et al., 2002, 1998). Considering its elastic nature, localized incorporation of TNC at branch tips may increase the compliance of the mesenchyme to facilitate epithelial extension.

Here, we present a mechanistic model for airway branching morphogenesis in the avian embryonic lung. Epithelial cells undergo apical constriction to initiate branching and simultaneously activate FAK. Activated FAK is necessary for epithelial synthesis of TNC. After branching is initiated, both the basement membrane and the mesenchymal ECM are actively remodeled. Basement membrane thinning at the branch tip facilitates branch extension and requires mesenchymally derived MMP2. As the epithelium extends, the adjacent mesenchymal cells change shape, which corresponds to a local increase in fluidity of the mesenchyme and transport of TNC from the epithelial surface deeper into the stroma. Therefore, dynamic and reciprocal interactions between the epithelium and mesenchyme remodel the ECM and promote airway branching morphogenesis in the embryonic chicken lung.

MATERIALS AND METHODS

Ex vivo culture of embryonic chicken lungs

Fertilized White Leghorn chicken (*Gallus gallus* variant *domesticus*) eggs were obtained from Hyline International. All experiments with embryonated eggs complied with ethical regulations for the care and use of animals, as approved by the Princeton University Institutional Animal Care and Use Committee. Eggs were incubated at 37°C until the desired developmental stage. Embryonic lungs were dissected in sterilized PBS. Lung explants were transferred to Nuclepore Track-Etch membranes (25 mm diameter, 0.8 µm pore size, Whatman) in DMEM/F12 medium (without HEPES) containing 5% fetal bovine serum (FBS, Atlanta Biologicals) and 50 units/ml penicillin/streptomycin (Invitrogen), as described previously (Gleghorn et al., 2012; Kim et al., 2013). Small molecule inhibitors of FAK (PF-573228, Sigma) and MMPs (GM6001, Calbiochem; batimastat, Tocris; ARP100, Tocris; MMP2i-II, Calbiochem) were added to the culture medium and explants were imaged under bright field using an inverted microscope (Nikon).

RNA extraction, library construction and sequencing

Total RNA was isolated from chicken lungs freshly dissected at embryonic day (E)5 (HH25-HH27) or E6 (HH28-HH29) using the RNeasy Fibrous Tissue Mini kit (Qiagen). Library construction for RNA sequencing was performed using the TruSeq Stranded mRNA Sample Preparation Guide, Low Sample (LS) protocol according to the manufacturer's instructions (Illumina). Sequencing was performed using the Illumina HiSeq 2000 Platform at the Lewis Sigler Institute for Integrative Genomics sequencing facility, using three independent samples for each time point (E5 and E6). The dataset was analyzed using DESeq2 package and gene ontology (GO) analysis was performed using the GSEA software package, referencing Ensembl genome Gallus_gallus-4.0 for gene annotation. All GO sets with a $P<0.05$ are listed in Table S1.

Mesenchyme-free culture

Lungs dissected from HH28-HH29 embryos were incubated in 10 U/ml dispase for 20 min at room temperature and the mesenchyme was removed using fine tungsten needles. Denuded airway epithelium was then embedded in Matrigel (BD Biosciences) and cultured in DMEM/F12 medium supplemented with 5% FBS and 150 ng/ml fibroblast growth factor 1 (FGF1; R&D Systems). Mesenchyme-free epithelium was cultured for 24 h and then either fixed in 4% paraformaldehyde (PFA) and immunostained for TNC and E-cadherin, or transferred to Trizol (Invitrogen) for RNA isolation, Verso cDNA synthesis (Thermo Fisher Scientific) and qPCR (iTaq SYBR Green Supermix, Bio-Rad) analysis following manufacturers' protocols.

Immunohistochemistry

For whole-mount analysis, lungs were fixed for 15 min in 4% PFA at room temperature and immunostained following standard procedures. For sectioned immunohistochemistry, lungs were fixed in 4% PFA overnight at 4°C, then perfused with 5% and 15% (w/v) sucrose in PBS and embedded in 7.5% (w/v) gelatin containing 15% (w/v) sucrose. Lungs were cryosectioned into 14 µm sections and prepared for immunostaining using standard protocols. The following primary antibodies were used at 1:30 dilution in antibody buffer [PBS containing 0.1% Triton X-100, 5% heat-inactivated goat serum (Atlanta Biologics) and 0.1% bovine serum albumin (BSA)]: mouse anti-laminin [31/31-2; IgG1; Developmental Studies Hybridoma Bank (DSHB)], mouse anti-perlecan (5C9; IgG1; DSHB), mouse anti-fibronectin [VA1(3); IgG1; DSHB] and mouse anti-TN (M1-B4; IgG1; DSHB). The M1-B4 TN antibody is a polyclonal antibody that detects multiple tenascin proteins; however, only TNC was detected in the chicken lung. For simplicity, we refer to the protein labeled by the M1-B4 antibody as TNC. Mouse anti-E-cadherin (1:200; IgG2a; BD Transduction Laboratories) or rabbit anti-cytokeratin (1:200; IgG; Agilent) were used to label airway epithelial cells. Rabbit anti-FAK (pY397) was used to label activated FAK (1:200; IgG; Invitrogen). The following secondary antibodies (Invitrogen) were used at 1:200: Alexa-647 goat anti-rabbit IgG, Alexa-594 goat anti-mouse IgG2a, Alexa-488 goat anti-mouse IgG1 and Alexa-594 goat anti-rabbit IgG. Slides were cover-slipped with Perma Fluor (Thermo Fisher Scientific). Whole-mount immunostained tissues were cleared in glycerol. Lungs used for phalloidin staining were fixed in 4% PFA supplemented with 0.25% glutaraldehyde for 15 min at room temperature and were labeled with phalloidin 594 (1:200; Invitrogen) overnight at 4°C. Tissues were cleared by first dehydrating in a graded isopropanol wash series, followed by perfusion with Murray's clear (1:2 ratio of benzyl alcohol:benzyl benzoate; Sigma). Fluorescent images were captured using a spinning disk confocal (BD CARV II, Biosciences) attached to an inverted microscope (Nikon Ti).

EdU analysis

Proliferating cells were detected with the Click-iT EdU Imaging kit (Invitrogen). Cultured explants were pulsed with 5-ethynyl-2′-deoxyuridine (EdU) for 30 min and then fixed in 4% paraformaldehyde. AlexaFluor-azide was used to visualize EdU^+ cells following the manufacturer's protocol.

Development (2019) 146, dev175257. doi:10.1242/dev.175257

Explants were then immunostained for E-cadherin as described above to determine the number of EdU^+ cells within the airway epithelium.

qRT-PCR analysis

Total RNA was isolated from explanted tissue following standard Trizol extraction (Invitrogen). Reverse transcription of RNA was performed using the Verso cDNA synthesis kit (Thermo Fisher Scientific) according to the manufacturer's protocol. qRT-PCR was conducted on a StepOnePlus Real-time PCR System (Applied Biosystems) using iTaq Universal SYBR Green SuperMix (Bio-Rad). To validate gene expression observed in the RNA-Seq, each target gene was normalized to that of 18S ribosomal RNA (Kuchipudi et al., 2012). Differential gene expression in explanted lungs was normalized to that of GAPDH using previously published primers (Spurlin and Lwigale, 2013). The primers used for qRT-PCR are listed in Table S2.

Analysis of basement membrane staining intensity

Measurements of protein distribution and staining intensity were performed using the ImageJ line measurement tool. The width of the selection line was adjusted to span the width of staining, and this was held constant for all images of the same stain. Basement membrane levels were measured by tracing the basal surface of the dorsal airway epithelium. Intensity of mesenchymal protein was measured by drawing the line selection through 30 µm of mesenchyme directly proximal to the tip of the *b1* branch between 0.2-0.7 of the total length of the branch surface.

Protein isolation and western blotting

After culturing explanted lungs, 10-12 lungs were pooled together for each independent sample. Samples were homogenized in 3× Laemmli lysis buffer and protein concentrations were measured using the Pierce bicinchoninic acid (BCA) Protein Assay Kit (Thermo Fisher Scientific). Samples were then mixed with bromophenol blue, boiled at 95°C for 5 min and resolved by electrophoresis on a 4-12% gradient SDS-PAGE gel in non-reducing conditions. Proteins were then transferred onto nitrocellulose membranes, which were blocked in 5% nonfat milk for 1 h at room temperature and incubated overnight at 4°C in blocking buffer containing antibodies to detect TNC (1:100; DSHB) or GAPDH (1:2000; Cell Signaling). Gels were imaged using a FluorChem E gel imaging system (Cell Biosciences).

Cell segmentation and heat map analysis

Cell shape was identified by staining lungs for F-actin. For whole-mount lungs, confocal stacks were generated with 0.5 µm *z*-resolution. An optical section from the center of the branch was selected and used for analysis. All images were subjected to background subtraction. Because F-actin labels cell boundaries, images were inverted to visualize cell shape. The 'analyze particle tool' in ImageJ was used to trace cells and compute aspect ratio (cell length/width). Heat maps of the aspect ratio of mesenchymal cells around the surface of epithelial branches were generated using a custom script in MATLAB. In brief, segmented cells around the branch tip were assigned coordinates of distance from the branch surface and relative arc position along the branch surface (where 0.0 is the proximal base and 1.0 is the distal base of the branch, Fig. S9). Branches of similar length were grouped together (binned by 30 µm branch length) to generate an average contoured branch surface. Respective average deformation in the mesenchyme was then fit to the average contour of the branch surface. Magnitude of cell deformation was measured by computing average cell aspect ratio within a constant area of mesenchyme (2100 μm^2) centered at the tip of b1 branches during various stages of extension.

In situ hybridization

Riboprobes for *in situ* hybridization analysis were generated by amplifying a target gene fragment from a HH28 lung cDNA pool. Individual gene fragments were cloned into TOPO-PCRII (Invitrogen) and digoxigenin (DIG)-labeled riboprobes were synthesized by *in vitro* RNA transcription reaction (Sigma). The primers used to generate these probes are listed in Table S2. Sense negative controls were hybridized in parallel for each gene. Isolated lungs were fixed overnight in 4% PFA and stored at −20°C in 100% methanol until use. Prior to hybridization, lungs were rehydrated in diethyl pyrocarbonate (DEPC)-treated PBS containing 0.01% Tween-20 and digested with proteinase K (10 µg/ml; Thermo Fisher Scientific) for 10 min at room temperature. Tissue digestion was terminated by re-fixation of lungs with 4% PFA in DEPC-PBS supplemented with 0.01% glutaraldehyde for 15 min. Tissues were then hybridized with riboprobe at 58.5°C overnight. After hybridization, probes were detected with anti-DIG antibody conjugated with alkaline phosphatase (Sigma) and color was developed with 5-bromo-4-chloro-3-indolyl phosphate/nitro blue tetrazolium (BCIP/NBT; Sigma), according to the manufacturer's instructions. Following color development, lungs were fixed with 4% PFA, cleared in glycerol and imaged using an OMAX A35140U digital microscope camera mounted on a dissection stereomicroscope (Olympus).

Blood vessel labeling

Blood vessels in the developing lungs were labeled by injecting the extra-embryonic vitelline vasculature of staged chicken embryos with 20 µl of 2 mg/ml fluorescein-conjugated lectin isolated from *Sambucus nigra* (Vector Laboratories). Lungs were then isolated and immunostained as described above.

Particle injection and tracking

Pulled glass needles were used to inject 1 µm diameter carboxylate-modified latex FluoroSpheres (excitation: 580 nm, Invitrogen) into intact explanted lung mesenchyme surrounding the tip of b1 or adjacent to non-branching regions. Lung explants were cultured on Falcon Cell Culture transwell inserts (353181, Corning) within 12-well tissue culture plates. Timelapse imaging was performed using a stage-top incubator held at 37°C, 5% CO_2 and 90% relative humidity (Pathology Devices). *Z*-stack images (20 µm) were collected every 30 min. A timelapse video was generated from the center-most *z* position of each branch. Beads were identified and tracked using the 2D particle tracking plug-in within the FIJI/ImageJ MosaicSuite (Sbalzarini and Koumoutsakos, 2005). A minimum of 10 representative beads from each timelapse video were analyzed. Tracks were only considered if the bead was continuously tracked for at least 7.5 h. The time- and ensemble-averaged mean squared displacement (MSD) of beads was calculated using Eqn 1. MSD data were fit to a power-law model in order to estimate the slope:

$$MSD(\tau) = \langle (x(t+\tau) - x(t))^2 \rangle + \langle (y(t+\tau) - y(t))^2 \rangle. \quad (1)$$

Statistical analysis

Statistical analysis was completed using GraphPad statistical tools. Student's *t*-test was used for any comparisons between one condition and its control. One-way ANOVA with Tukey multiple comparison post-hoc test was used for all other data analysis.

Acknowledgements

The authors would like to thank the members of the Tissue Morphodynamics Group for helpful discussions.

Competing interests

The authors declare no competing or financial interests.

Author contributions

Conceptualization: J.W.S., C.M.N.; Methodology: J.W.S., M.J.S., B.A.N.; Formal analysis: J.W.S.; Investigation: J.W.S., M.J.S., B.A.N., M.-F.P., S.J., R.Z.; Writing - original draft: J.W.S.; Writing - review & editing: C.M.N.; Supervision: C.M.N.; Project administration: C.M.N.; Funding acquisition: C.M.N.

Funding

This work was supported in part by grants from the National Institutes of Health (HL118532, HL120142 and CA187692), the National Science Foundation (CMMI-1435853), the David and Lucile Packard Foundation, the Camille and Henry Dreyfus Foundation, and the Burroughs Wellcome Fund. J.W.S. was supported in part by an National Research Service Award Postdoctoral Fellowship (HL137273). M.J.S. was supported in part by the National Science Foundation Graduate

Research Fellowship Program and the Wallace Memorial Fellowship in Engineering. B.A.N. was supported in part by a postgraduate scholarship-doctoral (PGS-D) from the Natural Sciences and Engineering Research Council of Canada. M.F.P. was supported in part by postdoctoral fellowships from the Svenska Sällskapet för Medicinsk Forskning (SSMF) and the New Jersey Commission on Cancer Research (NJCCR). C.M.N. was supported in part by a Faculty Scholars Award from the Howard Hughes Medical Institute. Deposited in PMC for release after 12 months.

Data availability

The RNA-Seq datasets have been deposited in GEO under accession number GSE132478.

Supplementary information

Supplementary information available online at
http://dev.biologists.org/lookup/doi/10.1242/dev.175257.supplemental

References

Abbott, L. A., Lester, S. M. and Erickson, C. A. (1991). Changes in mesenchymal cell-shape, matrix collagen and tenascin accompany bud formation in the early chick lung. *Anat. Embryol.* **183**, 299-311. doi:10.1007/BF00192217

Aufderheide, E. and Ekblom, P. (1988). Tenascin during gut development: appearance in the mesenchyme, shift in molecular forms, and dependence on epithelial-mesenchymal interactions. *J. Cell Biol.* **107**, 2341-2349. doi:10.1083/jcb.107.6.2341

Aufderheide, E., Chiquet-Ehrismann, R. and Ekblom, P. (1987). Epithelial-mesenchymal interactions in the developing kidney lead to expression of tenascin in the mesenchyme. *J. Cell Biol.* **105**, 599-608. doi:10.1083/jcb.105.1.599

Belanger, I. and Beaulieu, J. F. (2000). Tenascin in the developing and adult human intestine. *Histol. Histopathol.* **15**, 577-585.

Bellusci, S., Grindley, J., Emoto, H., Itoh, N. and Hogan, B. L. (1997). Fibroblast growth factor 10 (FGF10) and branching morphogenesis in the embryonic mouse lung. *Development* **124**, 4867-4878.

Bi, D., Yang, X., Marchetti, M. C. and Manning, M. L. (2016). Motility-driven glass and jamming transitions in biological tissues. *Phys. Rev. X* **6**, 021011. doi:10.1103/PhysRevX.6.021011

Bonnans, C., Chou, J. and Werb, Z. (2014). Remodelling the extracellular matrix in development and disease. *Nat. Rev. Mol. Cell Biol.* **15**, 786-801. doi:10.1038/nrm3904

Cao, Y. and Li, H. (2006). Single molecule force spectroscopy reveals a weakly populated microstate of the FnIII domains of tenascin. *J. Mol. Biol.* **361**, 372-381. doi:10.1016/j.jmb.2006.06.014

Cardoso, W. V. and Lu, J. (2006). Regulation of early lung morphogenesis: questions, facts and controversies. *Development* **133**, 1611-1624. doi:10.1242/dev.02310

Chen, W. T., Chen, J. M. and Mueller, S. C. (1986). Coupled expression and colocalization of 140K cell adhesion molecules, fibronectin, and laminin during morphogenesis and cytodifferentiation of chick lung cells. *J. Cell Biol.* **103**, 1073-1090. doi:10.1083/jcb.103.3.1073

Chiquet, M., Matthisson, M., Koch, M., Tannheimer, M. and Chiquet-Ehrismann, R. (1996). Regulation of extracellular matrix synthesis by mechanical stress. *Biochem. Cell Biol.* **74**, 737-744. doi:10.1139/o96-080

Chiquet-Ehrismann, R. and Chiquet, M. (2003). Tenascins: regulation and putative functions during pathological stress. *J. Pathol.* **200**, 488-499. doi:10.1002/path.1415

Chiquet-Ehrismann, R., Kalla, P., Pearson, C. A., Beck, K. and Chiquet, M. (1988). Tenascin interferes with fibronectin action. *Cell* **53**, 383-390. doi:10.1016/0092-8674(88)90158-4

Chiquet-Ehrismann, R., Tannheimer, M., Koch, M., Brunner, A., Spring, J., Martin, D., Baumgartner, S. and Chiquet, M. (1994). Tenascin-C expression by fibroblasts is elevated in stressed collagen gels. *J. Cell Biol.* **127**, 2093-2101. doi:10.1083/jcb.127.6.2093

Cohen, E. D., Ihida-Stansbury, K., Lu, M. M., Panettieri, R. A., Jones, P. L. and Morrisey, E. E. (2009). Wnt signaling regulates smooth muscle precursor development in the mouse lung via a tenascin C/PDGFR pathway. *J. Clin. Invest.* **119**, 2538-2549. doi:10.1172/JCI38079

Daley, W. P. and Yamada, K. M. (2013). ECM-modulated cellular dynamics as a driving force for tissue morphogenesis. *Curr. Opin. Genet. Dev.* **23**, 408-414. doi:10.1016/j.gde.2013.05.005

Danopoulos, S., Alonso, I., Thornton, M. E., Grubbs, B. H., Bellusci, S., Warburton, D. and Al Alam, D. (2018). Human lung branching morphogenesis is orchestrated by the spatiotemporal distribution of ACTA2, SOX2, and SOX9. *Am. J. Physiol. Lung Cell. Mol. Physiol.* **314**, L144-L149. doi:10.1152/ajplung.00379.2017

De Langhe, S. P., Sala, F. G., Del Moral, P.-M., Fairbanks, T. J., Yamada, K. M., Warburton, D., Burns, R. C. and Bellusci, S. (2005). Dickkopf-1 (DKK1) reveals that fibronectin is a major target of Wnt signaling in branching morphogenesis of the mouse embryonic lung. *Dev. Biol.* **277**, 316-331. doi:10.1016/j.ydbio.2004.09.023

Erickson, H. P. and Bourdon, M. A. (1989). Tenascin: an extracellular matrix protein prominent in specialized embryonic tissues and tumors. *Annu. Rev. Cell Biol.* **5**, 71-92. doi:10.1146/annurev.cb.05.110189.000443

Fata, J. E., Werb, Z. and Bissell, M. J. (2004). Regulation of mammary gland branching morphogenesis by the extracellular matrix and its remodeling enzymes. *Breast Cancer Res.* **6**, 1-11. doi:10.1186/bcr634

Fluck, M., Tunc-Civelek, V. and Chiquet, M. (2000). Rapid and reciprocal regulation of tenascin-C and tenascin-Y expression by loading of skeletal muscle. *J. Cell Sci.* **113**, 3583-3591.

Gebb, S. A., Fox, K., Vaughn, J., McKean, D. and Jones, P. L. (2005). Fetal oxygen tension promotes tenascin-C-dependent lung branching morphogenesis. *Dev. Dyn.* **234**, 1-10. doi:10.1002/dvdy.20500

Gleghorn, J. P., Kwak, J., Pavlovich, A. L. and Nelson, C. M. (2012). Inhibitory morphogens and monopodial branching of the embryonic chicken lung. *Dev. Dyn.* **241**, 852-862. doi:10.1002/dvdy.23771

Gomes, A. M., Bhat, R., Correia, A. L., Mott, J. D., Ilan, N., Vlodavsky, I., Pavao, M. S. and Bissell, M. (2015). Mammary branching morphogenesis requires reciprocal signaling by heparanase and MMP-14. *J. Cell. Biochem.* **116**, 1668-1679. doi:10.1002/jcb.25127

Guo, Y., Chen, T.-H., Zeng, X., Warburton, D., Boström, K. I., Ho, C.-M., Zhao, X. and Garfinkel, A. (2014). Branching patterns emerge in a mathematical model of the dynamics of lung development. *J. Physiol.* **592**, 313-324. doi:10.1113/jphysiol.2013.261099

Harunaga, J. S., Doyle, A. D. and Yamada, K. M. (2014). Local and global dynamics of the basement membrane during branching morphogenesis require protease activity and actomyosin contractility. *Dev. Biol.* **394**, 197-205. doi:10.1016/j.ydbio.2014.08.014

Hohenester, E. and Yurchenco, P. D. (2013). Laminins in basement membrane assembly. *Cell Adh. Migr.* **7**, 56-63. doi:10.4161/cam.21831

Iber, D. and Menshykau, D. (2013). The control of branching morphogenesis. *Open Biol.* **3**, 130088. doi:10.1098/rsob.130088

Imanaka-Yoshida, K., Yoshida, T. and Miyagawa-Tomita, S. (2014). Tenascin-C in development and disease of blood vessels. *Anat. Rec.* **297**, 1747-1757. doi:10.1002/ar.22985

Inaguma, Y., Kusakabe, M., Mackie, E. J., Pearson, C. A., Chiquet-Ehrismann, R. and Sakakura, T. (1988). Epithelial induction of stromal tenascin in the mouse mammary gland: from embryogenesis to carcinogenesis. *Dev. Biol.* **128**, 245-255. doi:10.1016/0012-1606(88)90288-6

Kim, H. Y. and Nelson, C. M. (2012). Extracellular matrix and cytoskeletal dynamics during branching morphogenesis. *Organogenesis* **8**, 56-64. doi:10.4161/org.19813

Kim, H. Y., Varner, V. D. and Nelson, C. M. (2013). Apical constriction initiates new bud formation during monopodial branching of the embryonic chicken lung. *Development* **140**, 3146-3155. doi:10.1242/dev.093682

Kim, H. Y., Pang, M.-F., Varner, V. D., Kojima, L., Miller, E., Radisky, D. C. and Nelson, C. M. (2015). Localized smooth muscle differentiation is essential for epithelial bifurcation during branching morphogenesis of the mammalian lung. *Dev. Cell* **34**, 719-726. doi:10.1016/j.devcel.2015.08.012

Kimmel, C. B., Ballard, W. W., Kimmel, S. R., Ullmann, B. and Schilling, T. F. (1995). Stages of embryonic development of the zebrafish. *Dev. Dyn.* **203**, 253-310. doi:10.1002/aja.1002030302

Kimura, T., Shiraishi, K., Furusho, A., Ito, S., Hirakata, S., Nishida, N., Yoshimura, K., Imanaka-Yoshida, K., Yoshida, T., Ikeda, Y. et al. (2014). Tenascin C protects aorta from acute dissection in mice. *Sci. Rep.* **4**, 4051. doi:10.1038/srep04051

Klotzsch, E., Smith, M. L., Kubow, K. E., Muntwyler, S., Little, W. C., Beyeler, F., Gourdon, D., Nelson, B. J. and Vogel, V. (2009). Fibronectin forms the most extensible biological fibers displaying switchable force-exposed cryptic binding sites. *Proc. Natl. Acad. Sci. USA* **106**, 18267-18272. doi:10.1073/pnas.0907518106

Koch, M., Wehrle-Haller, B., Baumgartner, S., Spring, J., Brubacher, D. and Chiquet, M. (1991). Epithelial synthesis of tenascin at tips of growing bronchi and graded accumulation in basement membrane and mesenchyme. *Exp. Cell Res.* **194**, 297-300. doi:10.1016/0014-4827(91)90368-5

Kuchipudi, S. V., Tellabati, M., Nelli, R. K., White, G. A., Perez, B. B., Sebastian, S., Slomka, M. J., Brookes, S. M., Brown, I. H., Dunham, S. P. et al. (2012). 18S rRNA is a reliable normalisation gene for real time PCR based on influenza virus infected cells. *Virol. J.* **9**, 230. doi:10.1186/1743-422X-9-230

Lebeche, D., Malpel, S. and Cardoso, W. V. (1999). Fibroblast growth factor interactions in the developing lung. *Mech. Dev.* **86**, 125-136. doi:10.1016/S0925-4773(99)00124-0

Lu, P., Takai, K., Weaver, V. M. and Werb, Z. (2011). Extracellular matrix degradation and remodeling in development and disease. *Cold Spring Harb. Perspect Biol.* **3**, a005058. doi:10.1101/cshperspect.a005058

Mailleux, A. A., Kelly, R., Veltmaat, J. M., De Langhe, S. P., Zaffran, S., Thiery, J. P. and Bellusci, S. (2005). Fgf10 expression identifies parabronchial smooth muscle cell progenitors and is required for their entry into the smooth muscle cell lineage. *Development* **132**, 2157-2166. doi:10.1242/dev.01795

Manning, M. L., Foty, R. A., Steinberg, M. S. and Schoetz, E. M. (2010). Coaction of intercellular adhesion and cortical tension specifies tissue surface tension. *Proc. Natl. Acad. Sci. USA* **107**, 12517-12522. doi:10.1073/pnas.1003743107

McKean, D. M., Sisbarro, L., Ilic, D., Kaplan-Alburquerque, N., Nemenoff, R., Weiser-Evans, M., Kern, M. J. and Jones, P. L. (2003). FAK induces expression of Prx1 to promote tenascin-C-dependent fibroblast migration. *J. Cell Biol.* **161**, 393-402. doi:10.1083/jcb.jcb.200302126

Mehr, D., Pardubsky, P. D., Martin, J. A. and Buckwalter, J. A. (2000). Tenascin-C in tendon regions subjected to compression. *J. Orthop. Res.* **18**, 537-545. doi:10.1002/jor.1100180405

Midwood, K. S. and Schwarzbauer, J. E. (2002). Tenascin-C modulates matrix contraction via focal adhesion kinase- and Rho-mediated signaling pathways. *Mol. Biol. Cell* **13**, 3601-3613. doi:10.1091/mbc.e02-05-0292

Midwood, K. S., Valenick, L. V., Hsia, H. C. and Schwarzbauer, J. E. (2004). Coregulation of fibronectin signaling and matrix contraction by tenascin-C and syndecan-4. *Mol. Biol. Cell* **15**, 5670-5677. doi:10.1091/mbc.e04-08-0759

Midwood, K. S., Chiquet, M., Tucker, R. P. and Orend, G. (2016). Tenascin-C at a glance. *J. Cell Sci.* **129**, 4321-4327. doi:10.1242/jcs.190546

Min, H., Danilenko, D. M., Scully, S. A., Bolon, B., Ring, B. D., Tarpley, J. E., DeRose, M. and Simonet, W. S. (1998). Fgf-10 is required for both limb and lung development and exhibits striking functional similarity to Drosophila branchless. *Genes Dev.* **12**, 3156-3161. doi:10.1101/gad.12.20.3156

Mongera, A., Rowghanian, P., Gustafson, H. J., Shelton, E., Kealhofer, D. A., Carn, E. K., Serwane, F., Lucio, A. A., Giammona, J. and Campas, O. (2018). A fluid-to-solid jamming transition underlies vertebrate body axis elongation. *Nature* **561**, 401-405. doi:10.1038/s41586-018-0479-2

Moore, K. A., Polte, T., Huang, S., Shi, B., Alsberg, E., Sunday, M. E. and Ingber, D. E. (2005). Control of basement membrane remodeling and epithelial branching morphogenesis in embryonic lung by Rho and cytoskeletal tension. *Dev. Dyn.* **232**, 268-281. doi:10.1002/dvdy.20237

Morrisey, E. E. and Hogan, B. L. (2010). Preparing for the first breath: genetic and cellular mechanisms in lung development. *Dev. Cell* **18**, 8-23. doi:10.1016/j.devcel.2009.12.010

Moura, R. S., Coutinho-Borges, J. P., Pacheco, A. P., Damota, P. O. and Correia-Pinto, J. (2011). FGF signaling pathway in the developing chick lung: expression and inhibition studies. *PLoS ONE* **6**, e17660. doi:10.1371/journal.pone.0017660

Oberhauser, A. F., Marszalek, P. E., Erickson, H. P. and Fernandez, J. M. (1998). The molecular elasticity of the extracellular matrix protein tenascin. *Nature* **393**, 181-185. doi:10.1038/30270

Oberhauser, A. F., Badilla-Fernandez, C., Carrion-Vazquez, M. and Fernandez, J. M. (2002). The mechanical hierarchies of fibronectin observed with single-molecule AFM. *J. Mol. Biol.* **319**, 433-447. doi:10.1016/S0022-2836(02)00306-6

Orend, G. and Chiquet-Ehrismann, R. (2006). Tenascin-C induced signaling in cancer. *Cancer Lett.* **244**, 143-163. doi:10.1016/j.canlet.2006.02.017

Park, W. Y., Miranda, B., Lebeche, D., Hashimoto, G. and Cardoso, W. V. (1998). FGF-10 is a chemotactic factor for distal epithelial buds during lung development. *Dev. Biol.* **201**, 125-134. doi:10.1006/dbio.1998.8994

Park, J.-A., Kim, J. H., Bi, D., Mitchel, J. A., Qazvini, N. T., Tantisira, K., Park, C. Y., McGill, M., Kim, S.-H., Gweon, B. et al. (2015). Unjamming and cell shape in the asthmatic airway epithelium. *Nat. Mater.* **14**, 1040-1048. doi:10.1038/nmat4357

Patel, V. N., Knox, S. M., Likar, K. M., Lathrop, C. A., Hossain, R., Eftekhari, S., Whitelock, J. M., Elkin, M., Vlodavsky, I. and Hoffman, M. P. (2007). Heparanase cleavage of perlecan heparan sulfate modulates FGF10 activity during ex vivo submandibular gland branching morphogenesis. *Development* **134**, 4177-4186. doi:10.1242/dev.011171

Redick, S. D. and Schwarzbauer, J. E. (1995). Rapid intracellular assembly of tenascin hexabrachions suggests a novel cotranslational process. *J. Cell Sci.* **108**, 1761-1769.

Riggins, K. S., Mernaugh, G., Su, Y., Quaranta, V., Koshikawa, N., Seiki, M., Pozzi, A. and Zent, R. (2010). MT1-MMP-mediated basement membrane remodeling modulates renal development. *Exp. Cell Res.* **316**, 2993-3005. doi:10.1016/j.yexcr.2010.08.003

Roth-Kleiner, M., Hirsch, E. and Schittny, J. C. (2004). Fetal lungs of tenascin-C-deficient mice grow well, but branch poorly in organ culture. *Am. J. Respir. Cell Mol. Biol.* **30**, 360-366. doi:10.1165/rcmb.2002-0266°C

Sarasa-Renedo, A., Tunc-Civelek, V. and Chiquet, M. (2006). Role of RhoA/ROCK-dependent actin contractility in the induction of tenascin-C by cyclic tensile strain. *Exp. Cell Res.* **312**, 1361-1370. doi:10.1016/j.yexcr.2005.12.025

Sbalzarini, I. F. and Koumoutsakos, P. (2005). Feature point tracking and trajectory analysis for video imaging in cell biology. *J. Struct. Biol.* **151**, 182-195. doi:10.1016/j.jsb.2005.06.002

Serwane, F., Mongera, A., Rowghanian, P., Kealhofer, D. A., Lucio, A. A., Hockenbery, Z. M. and Campas, O. (2017). In vivo quantification of spatially varying mechanical properties in developing tissues. *Nat. Methods* **14**, 181-186. doi:10.1038/nmeth.4101

Shyer, A. E., Huycke, T. R., Lee, C., Mahadevan, L. and Tabin, C. J. (2015). Bending gradients: how the intestinal stem cell gets its home. *Cell* **161**, 569-580. doi:10.1016/j.cell.2015.03.041

Slack-Davis, J. K., Martin, K. H., Tilghman, R. W., Iwanicki, M., Ung, E. J., Autry, C., Luzzio, M. J., Cooper, B., Kath, J. C., Roberts, W. G. et al. (2007). Cellular characterization of a novel focal adhesion kinase inhibitor. *J. Biol. Chem.* **282**, 14845-14852. doi:10.1074/jbc.M606695200

Soulintzi, N. and Zagris, N. (2007). Spatial and temporal expression of perlecan in the early chick embryo. *Cells Tissues Organs* **186**, 243-256. doi:10.1159/000107948

Spurlin, J. W., III and Lwigale, P. Y. (2013). Wounded embryonic corneas exhibit nonfibrotic regeneration and complete innervation. *Invest. Ophthalmol. Vis. Sci.* **54**, 6334-6344. doi:10.1167/iovs.13-12504

Sun, Z., Guo, S. S. and Fässler, R. (2016). Integrin-mediated mechanotransduction. *J. Cell Biol.* **215**, 445-456. doi:10.1083/jcb.201609037

Tzou, D., W. Spurlin, J., III, Pavlovich, A. L., Stewart, C. R., Gleghorn, J. P. and Nelson, C. M. (2016). Morphogenesis and morphometric scaling of lung airway development follows phylogeny in chicken, quail, and duck embryos. *Evodevo* **7**, 12. doi:10.1186/s13227-016-0049-3

Varner, V. D., Gleghorn, J. P., Miller, E., Radisky, D. C. and Nelson, C. M. (2015). Mechanically patterning the embryonic airway epithelium. *Proc. Natl. Acad. Sci. USA* **112**, 9230-9235. doi:10.1073/pnas.1504102112

Volckaert, T., Campbell, A., Dill, E., Li, C., Minoo, P. and De Langhe, S. (2013). Localized Fgf10 expression is not required for lung branching morphogenesis but prevents differentiation of epithelial progenitors. *Development* **140**, 3731-3742. doi:10.1242/dev.096560

Warburton, D., Bellusci, S., De Langhe, S., Del Moral, P.-M., Fleury, V., Mailleux, A., Tefft, D., Unbekandt, M., Wang, K. and Shi, W. (2005). Molecular mechanisms of early lung specification and branching morphogenesis. *Pediatr. Res.* **57**, 26R-37R. doi:10.1203/01.PDR.0000159570.01327.ED

Weaver, M., Batts, L. and Hogan, B. L. M. (2003). Tissue interactions pattern the mesenchyme of the embryonic mouse lung. *Dev. Biol.* **258**, 169-184. doi:10.1016/S0012-1606(03)00117-9

Wessells, N. K. (1970). Mammalian lung development: interactions in formation and morphogenesis of tracheal buds. *J. Exp. Zool.* **175**, 455-466. doi:10.1002/jez.1401750405

White, A. C., Xu, J., Yin, Y., Smith, C., Schmid, G. and Ornitz, D. M. (2006). FGF9 and SHH signaling coordinate lung growth and development through regulation of distinct mesenchymal domains. *Development* **133**, 1507-1517. doi:10.1242/dev.02313

Wiseman, B. S., Sternlicht, M. D., Lund, L. R., Alexander, C. M., Mott, J., Bissell, M. J., Soloway, P., Itohara, S. and Werb, Z. (2003). Site-specific inductive and inhibitory activities of MMP-2 and MMP-3 orchestrate mammary gland branching morphogenesis. *J. Cell Biol.* **162**, 1123-1133. doi:10.1083/jcb.200302090

Wu, J. E. and Santoro, S. A. (1996). Differential expression of integrin alpha subunits supports distinct roles during lung branching morphogenesis. *Dev. Dyn.* **206**, 169-181. doi:10.1002/(SICI)1097-0177(199606)206:2<169::AID-AJA6>3.0.CO;2-G

Young, S. L., Chang, L.-Y. and Erickson, H. P. (1994). Tenascin-C in rat lung: distribution, ontogeny and role in branching morphogenesis. *Dev. Biol.* **161**, 615-625. doi:10.1006/dbio.1994.1057